Enhanced clearing of *Candida* biofilms on 3D urothelial cell *in-vitro* model by lysozyme-functionalized Fluconazole-loaded shellac nanoparticles

Anheng Wang,[a] Paul Weldrick,[a] Leigh A. Madden,[b] Vesselin N. Paunov[c,]*

Abstract: Candida urinary tract biofilms are increasingly witnessed in nosocomial infections due to reduced immunity of patients and the hospital ecosystem. The indwelling devices utilized to support patients with urethral diseases that connect the unsterilized external environent with the internal environment of the patient are another significant source of urinary tract biofilm infections. Recently, nanoparticles (NPs)-associated therapeutics have gained traction in a number of areas, including fighting antibiotic-resistant bacterial biofilm infection. However, most studies on nanotherapeutics delivery have only been carried out in laboratory settings rather than in clinical trials due to the lack of precise in-vitro and in-vivo models for testing their efficiency. Here we develop a novel biofilm-infected 3D human urothelial cell culture model to test the efficiency of nanoparticles (NPs)-based antifungal therapeutics. The NPs wre designed based on shellac cores, loaded with Fluconazole and a coating of the cationic enzyme lysozyme. Our formulation of 0.2 wt% lysozyme-coated 0.02 wt% Fluconazole-loaded 0.2 wt% shellac NPs, sterically stabilised by 0.25 wt% Poloxamer 407, showed super-enhanced efficiency in removing Candida albicans biofilms formed on a 3D layer urothelial cell clusteroids. The NPs formulation exhibited low toxicity to the urothelial cells. This study provides a reliable in-vitro model for Candida urinary tract biofilm infections which could potentially replace animal models testing of such antifugal nanotechnologies. The reproducibility and availability of a well defined biofilm-infected 3D urothelial

cell culture model gives valuable insights about the formation and clearing of fungal bioilms and could accelerate the clinical use of antifungal nanotherapeutics.

[a]Department of Chemistry, University of Hull, Cottingham Road, Hull, HU67RX, UK

[b]Department of Biomedical Sciences, University of Hull, Hull, HU67RX, UK

* [c]Department of Chemistry, Nazarbayev University, 53 Kabanbay Batyr Avenue, Nursultan city, 010000, Kazakhstan. E-mail: vesselin.paunov@nu.edu.kz

Introduction

Urinary tract infections (UTIs) are one of the most common diseases in all age groups, consuming many medical resources.[1] UTIs are the most common in women, with the lifetime incidence exceeding 40 %.[2] UTIs can be divided into cystitis, pyelonephritis, and prostatitis based on the analysis of clinical symptoms and microbiological types.[3-5] The main sites of infection in these three types of the urinary tract are the lower urinary tract, upper urinary tract, and kidney or prostate.[6]

Candida urinary tract infections are relatively rare in healthy individuals but are more likely to occur in nosocomial infections.[7] This is highly associated with the patient's reduced immunity. The hospital ecosystem also contributes to the increased rate of urinary tract infections among patients. *Candida albicans* infections account for 42 percent of hospital-acquired urinary tract infections in infants.[8] Another primary source of nosocomial infection on the urinary tract are indwelling devices used to support patients encountered urethral diseases, such as catheters and stents.[9,10]

The relevance of biofilms to catheter-associated urinary tract infection (CAUTI) is that a foreign body, such as an indwelling urethral catheter, connecting a normally sterile, hydrated body site to the outside world will inevitably become colonized with microorganisms. Catheters or other indwelling devices used to sustain patients with urinary tract diseases connect the normal sterile body part to the unsterilized external environment, significantly increasing the risk of biofilm infection.[11-13] In contrast with bacteria or fungal cells in planktonic state, both bacteria and fungi tend to form an extracellular polymeric substance (EPS) to encapsulate their colony on the surface of indwelling devices as they proliferate to increase their structural strength and resistance to drugs.[14,15] This unique ecosystem, called a biofilm, enhances the production of DNA, RNA, polysaccharides, and proteins by higher cell-cell interaction.[16,17] The pathogens in a biofilm phenotype, which are intrinsically more resistant to antimicrobials, inhibit the efficiency of traditional antimicrobial therapeutics.[18,19] The absorption properties of the EPS and the excretion of extracellular enzymes additionally boost the colony antimicrobial resistance.

Recently, nanotechnology-based approaches have started to gain traction for creating new antimicrobial formulations and delivery systems that are able to penetrate the EPS of biofilms and kill multidrug-resistant microbial strains.[20-21] Existing nanoparticle therapies are mainly based on inorganic substances, polymers, and various macromolecules and small molecules have been shown useful in preventing the formation if biofilms.[22-25] These nanoparticles are typically manufactured by microfluidics, self-assembly, or mechanical stretching and exhibit controllable size, shape, and surface properties.[26-28]

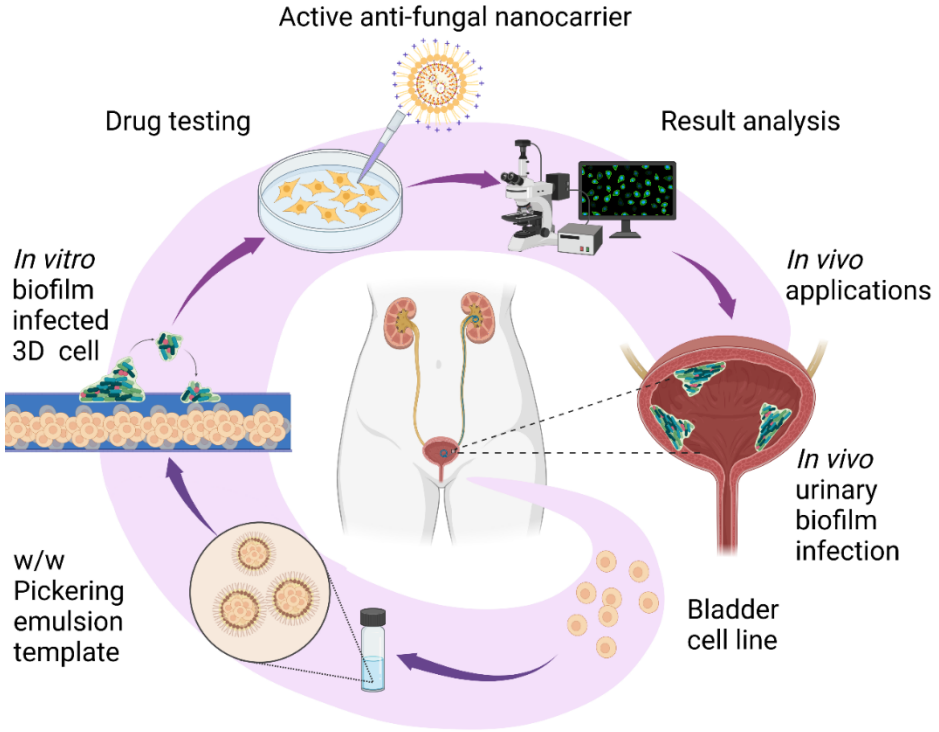

Figure 1. Schematic illustration of the in vitro 3D urinary cell model for testing anti-fungal nanotechnologies. Created with BioRender.com.

Recently, Polymeric antimicrobial nanocarriers,[46-50] metal-based nanocomposite[51-53], carbon-based nanomaterials, and dual functionalized nanoparticles have been developed a valuable nanotechnologies to enhance antimicibial effects and revive old antibiotics.

Increasing number of nanotechnology-based antimicrobials that hold promising potential against the threat of antibiotic-resistant biofilms in laboratory conditions.[24-30] It is worth mentioning that 99 % of existing nanotechnology-based antimicrobials will never be translated to clinical trials and used to benefit patients. One major issue that has dominated the nanotechnology field for many years is the lack of improvised *in vitro* testing platforms and animal models, which are essential before the clinical trial. Despite the safety and efficacy, animal models are often limited by their ethical and moral concerns. Existing *in vitro* models, such as 2D human cell culture, are too simplistic for biofilm simulation. More recently, literature has emerged that offers 3D cell culture, balancing the complexity of real organs and availability.[31,32] 3D cell cultures use microfluidics, extracellular matrix (ECM), or other devices to enhance cell-to-cell contact and produce organoids/spheroids cells with enhanced cell-to-cell signals and functionality.[33-35] These models are believed to be more advanced in simulating the *in-vivo* environment, and their cell cluster sizes (200 µm or larger) make it feasible to test the effect of drugs on a specific tissue. Research on this subject has been mostly limited to fabrication of spheroids with a very low yield which strongly inhibits its application in biomedical area.

Recently, the work describing using aqueous two phases system (APTS) water-in-water Pickering emulsion for the high throughput production of the spheroids emerged.[36] Several researchers have reported that this unique technology could

rapidly produce spheroids with considerable yield and enhanced functionality.[37,38] This opens the possibility for using a 3D urinary cell culture model to simulate the urinary fungal biofilm infection *in vitro.*

Here, we employed the cell line ECV 304, which is recognized as a mature bladder cell model with endothelial cells properties due to its high availability and stable phenotype, to produce 3D urinary cell clusteroids models using the ATPS based templating method.[36-38] We inoculated the 3D layer of urothelial cell clusteroids with a *Candida albicans* biofilm infection, followed by testing of the selected nanoformulation, Fluconazole-loaded Poloxamer 407 stabilised shellac nanoparticles, surface functionalized with Lysozyme, on its efficiency in clearing the biofilm. Note that the nanotechnology used here for the treatment of the fungal biofilm could be altered to any existing models. Here we use one of our established antifungal shellac nanocarrier systems with novel enzymatitic surface functionality of lysosyme and Fluconazole payload, as an example.

There are two primary aims of this study: (i) To investigate the feasibility of the fungal infection on 3D urinary cell models. (ii) To ascertain the efficiency of the selected nanotechnology for clearing fungal biofilms on 3D urinary cell layer. This study provides an exciting opportunity to advance the current *in vitro* models in simulating urinary track biofilm infection. The tested nanoformulation could prove effective for the downstream applications of the exceeding numbers of nanotechnologies.

We envisage that such nanoformulation could be used in future clinical studies for clearing fungal biofilms on bladder and utretra walls. Biofilms on the urotheluim could potentially be clinically targeted by delivering the dual functionalised nanoformulation into the bladder by catheter system through the urethra, where after clearing of the biofilm infection it woud naturally be excreted through the patient urinary tract. This nanotechnology may open the way of treating persistent fungal biofilm infections and the 3D urinary cell model is a good way of examining its effiency along with the testing of its biocompatibility with cells of the uretrium.

Materials and Methods

Materials

Shellac aqua solution (25 wt% aqueous suspensions) was sourced from SSB® AquaGold. The fungal species *Candida albicans* (Robin) Berkhout (ATCC MYA-2876) was obtained from ATCC. Poloxamer 407 (P407, analytic grade) and lysozyme powder (from hen egg white), poly-L-lysine, and sodium alginate were obtained from Sigma-Aldrich, UK. Whey protein was a gift from No 1 Supplements, Suffolk, UK. Dulbecco's Modified Eagle Medium, Corning® Transwell® polyester membrane cell culture inserts (96 microwell plates), 0.25 % trypsin-EDTA solutions, and NUNC Cell culture 6-well plates were bought from Thermo Fisher Scientific (UK). The RPMI 1604 medium (BE12-702F) supplemented with L-Glutamine for fungal cell culture was sourced from Lonza, Basel, Switzerland. Dextran (MW 500 kDa) and PEO (MW 200 kDa) were purchased from Alfa Saer, UK. Mueller-Hilton Broth (MHB), Mueller-Hilton Agar (MHA) were sourced from Oxford, UK. 10 %v/v Fetal bovine serum was from Labtech, Heathfield UK MTT kit was bought from Millipore Corp, U.S.A. Deionized water purified by the MilliQ water system (Millipore) was used in all experiments.

ECV 304 monolayer cell culture

The ECV 304 cell line is derived from human urinary bladder carcinoma which also represents many features of endothelial cells. This unique feature will make them a valuable model for the study of cellular processes in the urothelium/bladder cells behaviors and the cell-cell interactions. The dual cell characteristics combined with a fast proliferation rate also makes this cell line a ideal *in vitro* model for biofilm infection testing, as described below. The ECV 304 cell line was sourced from ECACC cell collection and was cultured in DMEM mediums supplemented with 10 % Fetal Bovine Serum (FBS) sources from Labtech, UK. The ECV 304 cells were incubated in T75 easYFlask (Fisher, UK) at 37 °C with 5 % CO_2 before the confluency reached 80 %. The medium was discarded and the cells were rinsed with phosphate buffer saline (PBS, Lonza, UK) twice to remove the excessive medium. The cells were passaged 1:8 using 0.25 wt% trypsin solution. The trypsinization was neutralized by adding a complete DMEM medium, and the cells were collected by centrifugation at 400 × g for 4 min.

Production of a 3D layer of ECV 304 cell clusteroids

The protocol of producing ECV 304 3D clusteroids was retouched from the method introduced by Das et. al.[36] Briefly, the protocol is based on an ATPS, water-in-water Pickering emulsion. 22 g PEO and 11 g dextran powders were suspended in 50 mL deionized water followed by autoclaving (121 °C , 15 min) to obtain 22 wt% PEO and 11 wt% DEX sterile solution. The 11 wt% PEO was blended with an equal volume of heat-treated whey protein particle (WPP) suspenion[36,37] before mixing with DMEM complete medium at a ratio of 1:1 to obtain 5.5 wt% PEO/DMEM/WPP solution. Similarly, a 5.5 wt% DEX solution was obtained in DMEM. The dextran phase (DEX) was used as the dispersed phase where the ECV 304 cells were initially affiliated to and altered to a fixed cell concentration (1×10^6/mL). The DEX and PEO phases were gently emulsified using a BD Plastipak™ syringe fitted with a BD Microlance™ 12 needle (21G 12, internal diameter 0.512 mm, BD biosciences, Wokingham, UK) by 6 pumps. After the DEX/PEO w/w Pickering emulsion was fabricated, the affiliation of the cells to the DEX phase would facilitate their encapsulation in the DEX droplets. The cells were compressed to form cell clusteroids by adding PEO/DMEM solution with higher concentration (11 wt%) to a final PEO concentration of 8 wt%. This causes a transfer of water from the DEX drops to the continuous PEO phase which shrinks the DEX drops along with the encapsulated cells. The w/w Pickering emulsions were incubated overnight to generate of clusteroids by increased cell-cell interations. The emulsions were diluted tenfold with a DMEM complete medium to enable the emulsion to break down and to allow sedimentation of the clusteroids by gravity. The clusteroids were then taken out and transferred to poly-L-lysine coated 6 well plates to produce a 3D layer of ECV 304 cell clusteroids. The culture was incubated with complete media at 37°C with 5% CO_2.

Preparation of *C.albicans* biofilm infected ECV 304 3D cell platform

A single colony of *C.* albicans was collectd with a plastic loop and seeded in a 10 mL Yeast Extract–Peptone–Dextrose (YPD) medium (Sigma-Aldrich, UK). The *C. albicans*-YPD suspension was incubated at 37°C for 12 h with stirring at 150 RPM. The overnight culture (O/N) was centrifugated at 1000×g for 5 min. The cells pellet was rinsed twice with sterile PBS solution to remove excess YPD medium before the *C. albicans* were reseeded in RPMI medium supplemented with 1 % L-glutamine. The fungal cell concentration was adjusted to 1×10^5/mL by series of dilutions using RPMI medium since this is the optimal condition for formation of Candida albicans biofilm. To monitor the spread of fungal infection, the *C. albicans* cells were stained using carboxyfluorescein succinimidyl ester (CFSE), which is a multi-generational dye that binds

to lysine residues and other amine sources. CFSE shows green signals under confocal microscopy or fluorescence microscopy set at the FITC channel (494 nm). The protocol for staining the fungal cells is given below. Briefly, a 10 mL aliquot of the C. *albicans* suspension with a fixed cell concentration of 1×10^5/mL was pelleted by centrifugation at 4000×g.

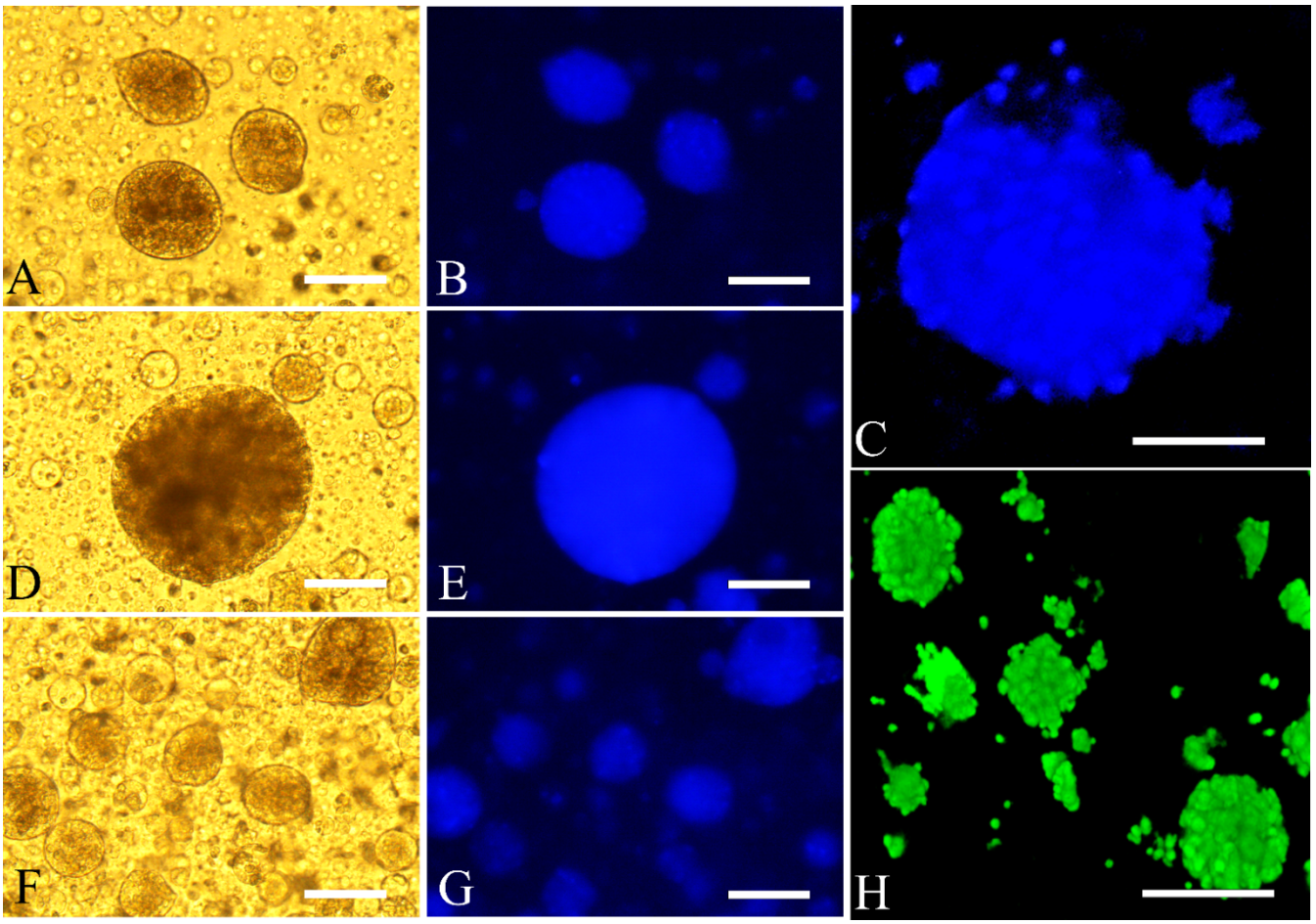

Figure 2. Optical brightfield microscopy images (A, D, F), fluorescence microscopy images (B, E, G, C), and confocal laser scanning microscope observation (E) of the individual ECV 304 cell clusteroids encapsulated in the w/w Pickering emulsions (5.5 wt % DEX,5.5 wt% PEO).[36,37] The clusteroids were stained with DAPI (B, E, G, C) or FDA live/dead assay (H). The bar is 50 µm for (A, B, D, E), 100 µm for (F, G), 50 µm for (C) and 200 µm for (H). The fluorescence intensity was measure by ZEN software (Blue edition).

The sediment was rinsed twice with sterilized PBS solution and resuspended in 2×CFSE working solution (20 µg CFSE in 10 ml PBS). The working suspension of *C. albicans* (labeled with CFSE or unlabeled) with optimal cell density was seeded to the formed 3D ECV304 cell clusteroids layer growing on the bottom of six well plates. Briefly, 20 µL of the *C. albicans* working suspension was added to each well. To allow the proliferating of the clusteroids, 200 µL DMEM complete medium was also pipetted into the wells. The plates were incubated *at* 37°C for 12 h to generate biofilm on the clusteroids layer. After the allotted time, the medium was discarded by gentle pipetting, and the clusteroids infected by biofilm adhered to

the wells were rinsed two times with sterilized PBS solution. DMEM medium was used for the cell culture and RPMI medium were for fungal cell culture.

Preparation of Fluconazole-loaded P407-stabilised shellac NPs

To prepare the NPs suspension, 200 µL of 25 wt% ammonium shellac solution (Aqua Gold) was diluted to 50 mL using deionized water to get 0.2 wt% ammonium shellac solution. Then 0.125 g of P407 and 0.01 g Fluconazole were added to the 0.2 wt% shellac solution followed by dropwise addition of 0.25M NaOH to change the pH to 10. This was followed by 30 min sonication using an ultrasonic bath (Ultrawave, U.K.) at 40 % of the maximum power of 200 at 25^{o}C and 30 min of magnetic stirring were conducted to solubilize the p407 and Fluconazole. The pH was then adjusted to 5.5 using 0.25M HCl solution to precipitate the individual components to shellc NPs. The final concentration of the 1×stock NPs formulation is 0.02 wt% Fluconazole-loaded 0.2 wt% Shellac NP sterically-stabilised with 0.25 wt% P407.

Coating of the Fluconazole-Loaded Shellac NPs with Lysozyme.

To functionalize the shellac nanoparticles with cationic surface functionality, 0.125 g of lysozyme powder was added to the 0.02 wt% Fluconazole-loaded 0.2 wt% Shellac NPs stabilized with 0.25 wt% P407 with agitation. The solution was sonicated for 15 min to avoid aggregation. The Lysozyme exhibits a very high positive charge at pH 5.5 and charge-reverse the originally anionic shellac NPs into cationic surface functionality by electrostatic binding. The Lysozyme-coated shellac NPs were collected by centrifugation at 8000×g for 30 min. The pelleted NPs were then resuspended in 50 mL deionized water to reach a final concentration of 0.02 wt% Fluconazole-loaded 0.2 wt% Shellac NPs stabilized by 0.25 wt% P407 and coated with 0.2 wt% Lysozyme. This concentration is treated as 1×stock suspension. To get more concentrated 2×, 3× or 4× suspension, the pelletized NPs were diluted in 25 mL, 16.7 mL, and 12.5 mL of deionized water, respectively.

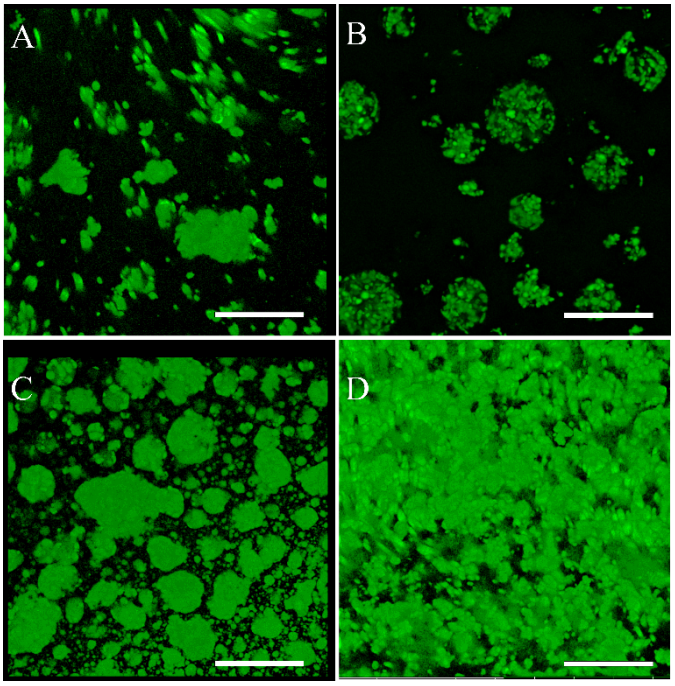

Figure 3.CLSM images of the proliferation of clusteroids layer at different days of culture: (A): day 1: (B): day 3; (C): day 5; (D): day 7. The initial cell number was normalized to 1 × 10^6 cells/mL. Zeiss LSM750 fluorescence microscope was employed to capture the images. The bar is 100 µm.

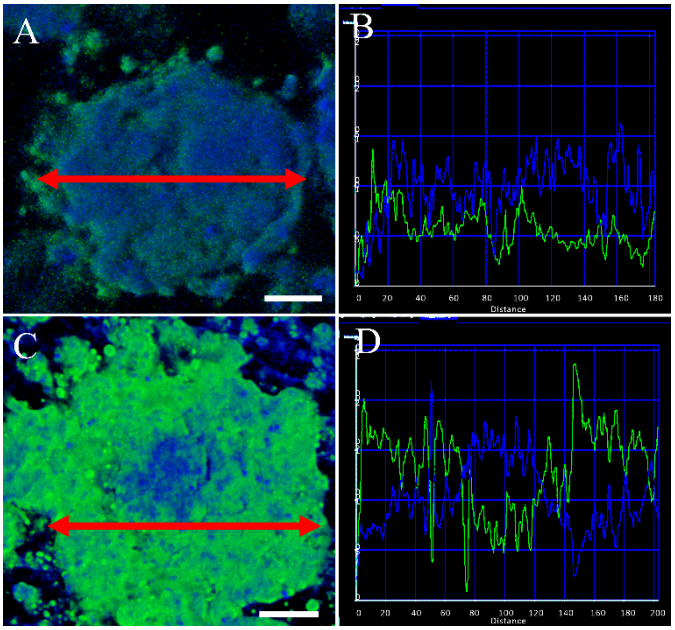

Figure 4. Confocal laser scanning microscope observation of individual ECV 304 clusteroids infected by *C. albicans* after A:1 h and C:24 h. The B and D show the fluorescence intensity of A and C, respectively. The bar is 50 µm. The red arrows indicate where the fluorescence intensity was measured.

Characterisation of Free Lysozyme, Lysozyme-coated shellac NPs, and Lysozyme-Coated Fluconazole-Loaded shellac NPs

Malvern Zetasizer Nano ZS was used to measure the zeta potential and particle size of the modified shellac NPs. The refractive index (RI) was set to 1.512, which is the RI of shellac. 1 mL of the samples was added to a quartz cuvette and tested three times at 25°C. The data was collected as a mean of three separate tests.

Bright field, fluorescence, and Confocal microscopy observations

The micro-structure of the individual clusteroids and the proliferation of the clusteroids collected from the DEX/PEO emulsion template were imaged with bright field optical microscopy supplemented with fluorescence microscopy (Olympus BX-51). 20 µL of the sample was carefully pipetted onto a concave slide at room temperature under various immersion objectives. To visualize the clusteroids, 4',6-diamidino-2-phenylindole (DAPI) was used as the fluorescence dye on the clusteroids before the clusteroids were observed. For tracking of the long-term proliferation of the clusteroids or the *C. albicans,* CFSE was used which would permeate into cells and bind to their interior by the succinimidyl group. The bacterial and the cells were pre-stained prior to the biofilm formation. For selective experiments, the clusteroids was

stained by CellTracker Green CMFDA (5-chloromethylfluorescein diacetate) and the *C. albicans* were stained with CFSE to allow monitoring over longer periods by fluorescence microscopy. The observation of the *C. albicans* biofilms and the 3D clusteroids co-culture model was carried out using Confocal Laser canning microscope (CLSM, Zeiss LSM710). Z-stacking images were taken to generate a 3D view of the biofilms on the clusteroids model, which composed 100 slices with 2 µm per slice. Two channels, 461 nm (DAPI) and 488 nm (FITC) were set at precise mode to avoid signal interference of the fluorescence signal within the stained ECV 304 cell clusteroids and *C. albicans biofilm*.

Biofilm clearance efficiency after the NPs treatment

After the biofilm-infected ECV 304 *in vitro* 3D model was obtained by the method mentioned above, the culture was firstly rinsed with PBS twice to remove any remaining planktonic fungal cells. The 1×standard stock solution was 0.02 wt% Fluconazole-loaded 0.2 wt% Shellac NP sterically-stabilised with 0.25 wt% P407. 100 µL of 1×, 2×, 3× and 4× stock suspensions were added separately to clusteroids/biofilm co-cultures and 100 µL of DMEM complete medium was supplemented to keep the cells proliferating. 0.1 mL of PBS with 0.2 mL DMEM complete medium was added to a well as control. The antibiofilm properties of the individual components of the NPs were also tested to prove the efficiency of the nanostructure. 100 µL of the prepared solutions of different individual components with an equal concentration in the NPs were also added into different well plates contained the biofilm/ECV 304 clusteroids co-cultures.

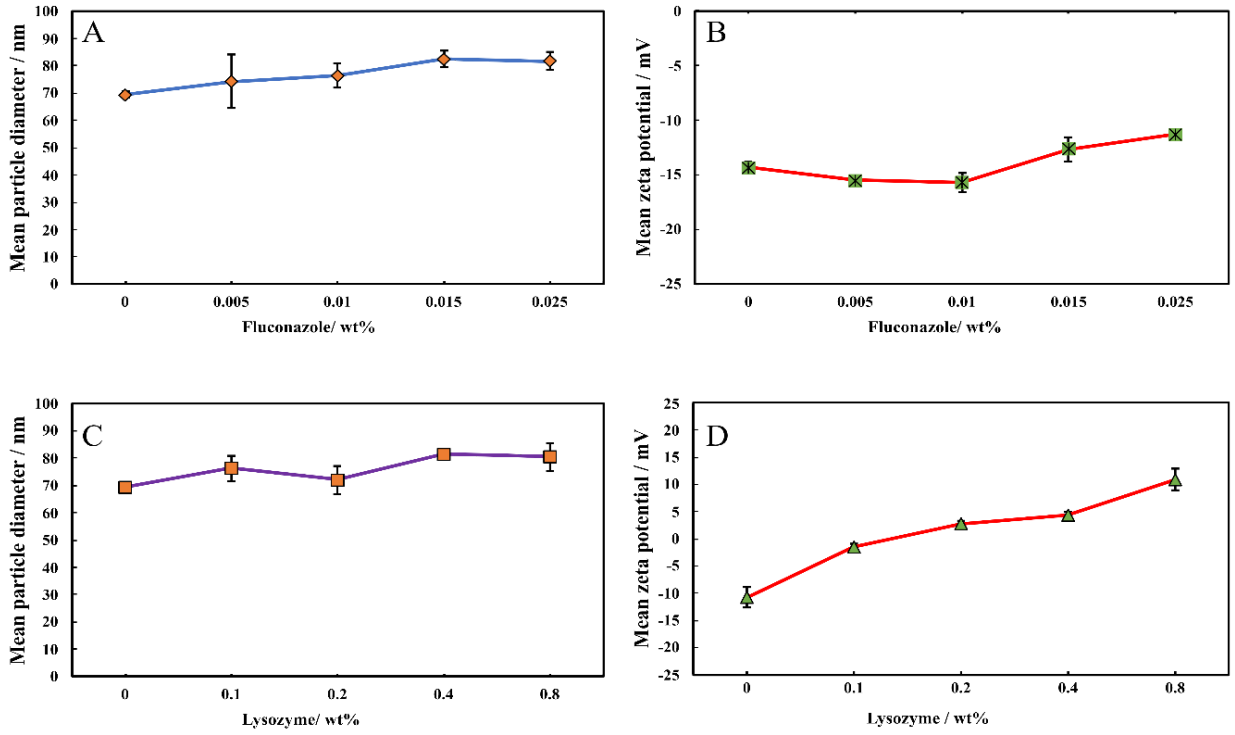

Figure 5. (A) Mean particle diameter of 0.2 wt% Shellac-0.25 wt% P407-Fluconazole nanoparticles measured at pH 5.5 (acetate buffered saline) with various concentrations of Fluconazole. (B) Mean particle zeta potential of 0.2 wt%

Shellac-0.25 wt% P407-Fluconazole nanoparticles versus the Fluconazole concentration. (C) Mean particle diameter vs. Lysozyme concentration of the 0.2 wt% Shellac-0.25 wt% P407-0.02 wt% Fluconazole-Lysozyme nanoparticles measured using a Malvern Zetasizer Nano ZS at 25 °C. Each value represents a triple replicate with ±S.D. (D) ζ-potential of 0.2 wt% Shella-0.25 wt% P407-0.02 wt% Fluconazole-Lysozyme nanoparticles immobilized with different concentrations of the Lysozyme at pH 5.5 (adjusted with acetate buffered saline) measured immediately after preparation.

After 24 hrs of treatment, the media was discarded and the cultures were collected and shaken for 30 secs with glass beads to release the fungal cells from the biofilm. The samples were then transfered to test tubes with 100 µL of fresh Mueller Hinton broth (MHB). Each example was vortexed for 30 secs to disassociate the biofilm and inoculate the MHB with bacterial cells. The drop plate count technique was utilized to quantify cell colony-forming unit (CFU)/mL. To gauge the fugal cell viability inside the biofilms, 10 × dilutions were made in MHB, 10 µL solutions were transferred onto MHA plates and left growing for 24 hours at 37°C. CFUs were checked from the last two droplets which contained a countable number of colonies (3 to 30 states for every 10 µL drop) and calculated as average.

Cytotoxicity test of the NPs treatment using MTT assay

The cytotoxicity of the NPs treatment on the ECV 304 cell clusteroids is a key feature in evaluating their potential to be used in clinical applications. The MTT assay was employed to test the ECV 304 cell viability after the clusteroids were imposed to the NPs treatment. The MTT is a colourimetric assay for evaluating the cell metabolic activity. Nicotinamide adenine dinucleotide phosphate (NADPH)-dependent cellular oxidoreductase enzymes may, under defined conditions, reflect the number of viable cells present. These enzymes are capable of reducing the tetrazolium dye 3-(4,5-dimethylthiazol-2-yl)-2,5-diphenyltetrazolium bromide to its insoluble formazan, which has a purple colour. 20 µL of Compound 1 was added to each microwell contained ECV 304 cells clusteroids with an initial cell number of about 5×10^5 supplemented with 100 µL DMEM complete medium, after 1 h and 24 h of cell incubation at 37° C with 5% CO_2, respectively. The Compound 1 was incubated with the cells for 30 min before removing the medium and adding 50 µL isopropanol. The microwell plates were then incubated for another 30 min and the then their absorbance at a wavelength of 490 nm was read into a microplate reader (BioTek Synergy HT).

SEM Imaging of shellac NPs, ECV 304 cells, and *C. albicans* biofilms on the ECV 304 3D clusteroirds layer

A samlle of the stock formulation of 0.02 wt% Fluconazole-loaded 0.2 wt% Shellac NPs stabilized by 0.25 wt% P407 and coated with 0.2 wt% Lysozyme was left to air dry before they were coated with gold for imaging. ECV 304 cells, *C. albicans* biofilm infected clusteroids, and NPs treated clusteroids/biofilm co-culture were gently collected from the well plate using a sterilized loop and shifted to glass slides. The cultures were fixed with 1 wt% glutaraldehyde in PBS buffer solution for 1 h at 25°C. The cultures were then rinsed three times with deionized water to wash away the excess of glutaraldehyde. Post-treatment, the 3D clusteroids were gently removed from the plate using a sterilised loop and placed onto a 7 mm diameter circular glass slide, and adhered to Carbon discs.

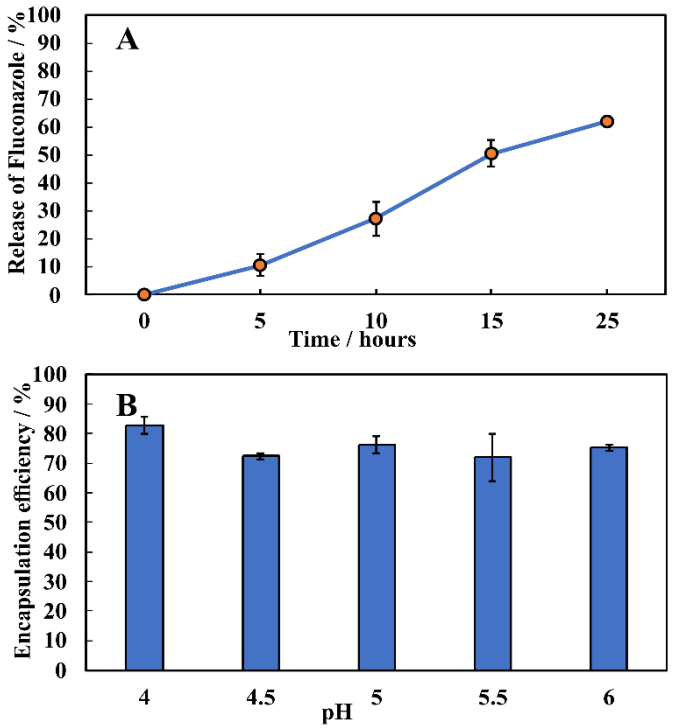

Figure 6. (A) Release of Fluconazole from 0.02 wt% Fluconazole-loaded 0.2 wt% Shellac NPs stabilized by 0.25 wt% P407 and coated with 0.2 wt% Lysozyme at different time points. (B) Encapsulation efficiency of 0.02 wt% Fluconazole-loaded 0.2 wt% Shellac NPs stabilized by 0.25 wt% P407 and coated with 0.2 wt% Lysozyme nanoparticles. The encapsulation efficiency was tested immediately after the NPs were prepared using a UV-visible spectrometry set at 260 nm wavelength. The lines are guides to the eye.

The biofilm was gently washed with deionized water to remove excess media and treatment. The biofilms were then fixed in a 1 wt% glutaraldehyde in PBS buffer solution for 1 h at room temperature. After fixation, the biofilms were washed 3 times with deionized water to remove excess glutaraldehyde. Samples were imaged with Zeiss smart SEM software (Zeiss Evo-60 S.E.M., Germany). The SEM images were processed with false colour to distinguish cells from biofilms (yellow colour for cells, green for *C. albicans* biofilm).

Cryostat sectioning

For the characterisation of the fungal infection inside the clusteroids layer, the *C. albicans* infected layer of ECV 304 clusteroids culture was detached from the microwell plate by a sterilized loop and placed on a filter paper. The culture was then frozen in the optimal cutting temperature compound overnight before serial cryostat sectioning. Leica CM1950 was used to create slices with a thickness of 10 µm, and the slice in the central region was collected and moved on to the glass slide. Olympus BX51 fluorescence microscope was used to visualize the sectioned slice.

Results and discussion

Preparation of ECV304 clusteroids and 3D clusteroids layer

The ECV 304 cells were harvested after the 2D cell monolayer culture reached 80% confluency after which they were moved to the DEX/PEO w/w Pickering emulsion template stabilized by 2 wt% whey protein particles. The cells were compacted in the droplets by adding a PEO solution of a higher concentration. The shrinking process would provide increased cell-cell adhesion and induce the formation of clusteroids (Figure S1). Notably, the concentration of the PEO/DEX and the shrinking process are essential in clusteroids formation which was proved in our former works. The clusteroids were left in the w/w Pickering emulsion for 12 h to allow cell interaction and adherence, after which they were collected by diluting the emulsion with 10 folds PBS as shown in Figure 1. Typical ECV 304 clusteroids collected from the w/w emulsions are shown in Figure S2. The SEM images compared the individual ECV 304 cells with clusteroids of ECV 304 cells, which clearly shows the microstructure of the cells within (Figure S2A,B). The collected clusteroids were stained with DAPI and FDA to preliminarily assess their integrity and viability. The production process based on the ATPS did not excert an adverse impact on the viability of the cells in the clusteroids as shown in Figure S3. A fixed amount of (1×10^5/mL cells) as collected clusteroids were then moved to 96 microwell plates precoated with poly-L-lysine as the substrate to allow the formation of clusteroids layer on the bottom of the wells. The growth of the clusteroids was continually monitored by CMFDA cell labelling which is a generational dye for living cell tracking. The results, as shown in Figure 3 and Figure S4, indicate that the clusteroids would proliferate fast and fuse into a dense 3D clusteroids layer which would potentially work as a proxy for the bladder inner urothelial cell wall within 7 days. The individual clusteroids firstly grew until the space between them was occupied, then the clusteroids started fuzzing into a tissue-like 3D compacted layer. The fusion of the clusteroids was shown in Figure S4. Overall, these results indicate that our w/w Pickering emulsion template would be an ideal platform for the fast preparation of such realistic in-vitro environment which can be further explored after biofilm infection and treatment.

***C. albicans* infection and formation of biofilm on top of the ECV 304 3D clusteroids layer**

The purpose here was to determine the biofilm formation on our simulated bladder inner urothelial wall model. The biofilm formation mechanism on implanted devices and the surface of various substrates has been well established and studied,[39,40] including tissues and implanted devices.[41-45] Our previous work has successfully demonstrated the *S. aureus* and *P. aeruginosa* biofilm formation on keratinocytes clusteroids.[27] The formation of biofilm on an *in-vitro* bladder wall model has not yet been explored up to our best knowledge. In order to assess the biofilm-infected 3D clusteroids layer model, a confocal microscopy observation was employed to confirm that whether *C. albicans* could successfully embed on the 3D clusteroid layer (Figure 4). The invasion of the fungal cells into individual cell clusteroids was clearly shown in Figure 4. After one hour of incubation, the fungal cells started to proliferate and surround the ENV 304 clusteroids.

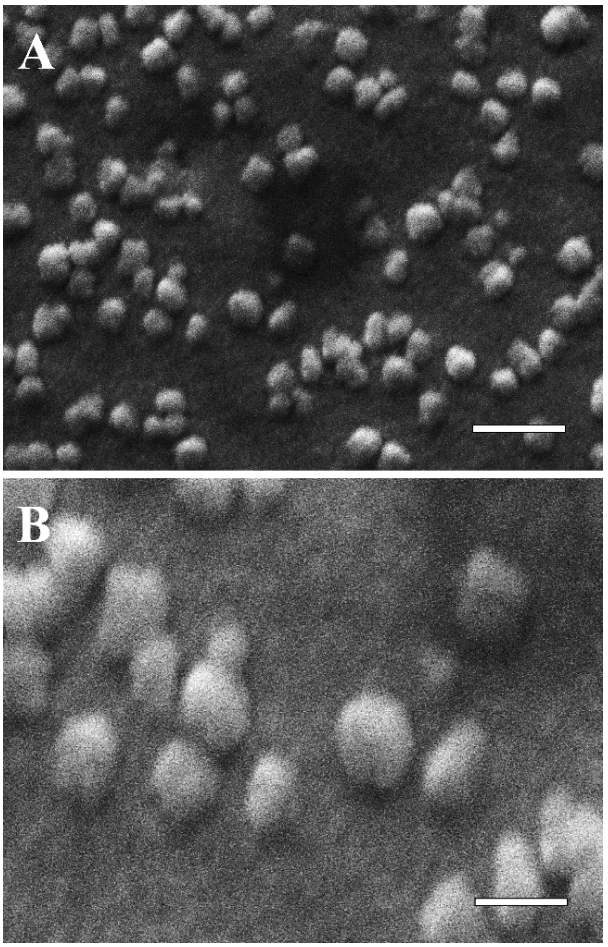

Figure 7. SEM observation of 0.25 wt% P407-stabilized 0.02 wt% Fluconazole-loaded 0.2 wt% Lysozyme coated 0.2 wt% shellac nanoparticles. The bar is 500 µm for (A) and and 100 µm for (B).

The difference between the "1 h" and "24 h" groups was significant; the fluorescence signals were dominated by the green FITC channel, which indicates the coverage of fungal cells on the layer of clusteroids and the formation of a biofilm. Similarly, the build-up of *C. albicans* biofilm above the 3D clusteroids layer was also investigated using CLSM (Figure S5). After 24 h one can also observe the biofilm generation on the clusteroids layer, which correlates with the result of the fluorescence microscopy. The specific morphology of the *C. albicans* biofilm on the ECV 304 cells clusteroids and the 3D clusteroids layer was further observed using SEM. As shown in Figures 9C and 9D, the individual *C. albicans* cells have an oval shape and prouces a thick aggregated layer on top of the ECV 304 clusteroids. Note that the formation of the biofilm does not disintegrate the structure of the cell clusteroids, although they are known to contaminate and detach 2D monolayers of cultured cell on solid substrates.

Preparation of the Fluconazole-loaded Shellac NPs and encapsulation efficiency test

The design of the NPs used in the current work is based on shellac core and P407. The fabrication of the current NPs was systematically studied in the work done by Al-Obaidy et al. [46,47] and Weldrick et al.[29]

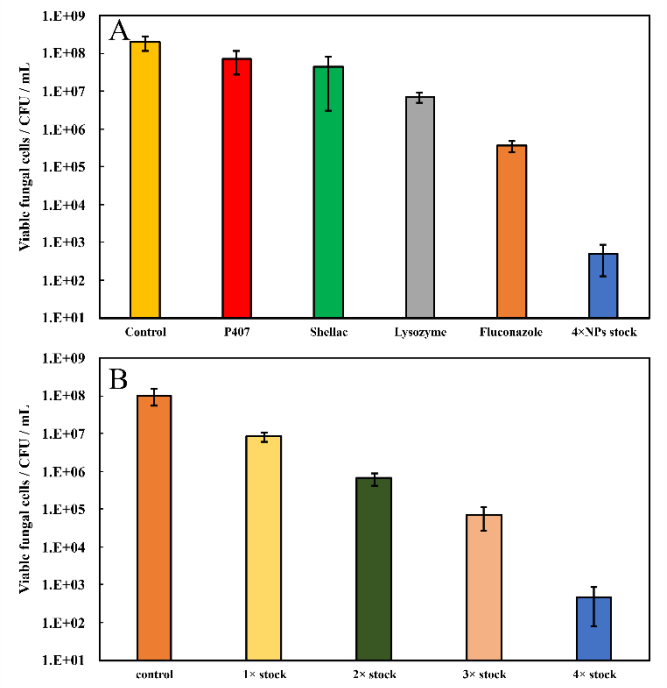

Figure 8. A: Efficiency of equavilant Individual components of the 4×stock NPs solution on of the clearance of C. albicans biofilm infected on the 3D culture of ECV 304 cell clusteroid layer. The fungal cell numbers were normalized by CFU B: Influence of different concentrations of the Lysozyme-coated Fluconazole-loaded Shellac NPs the on the proliferation of the 3D culture of ECV304 clusteroid layer after 1 h and 48 h culture. The concentration of the 1×standard stock solution is 0.2 wt% Shellac, 0.25 wt% P407, 0.2 wt% Lysozyme and 0.02 wt% Fluconazole.

The optimal precipitation conditions for such shellac NPs were found at pH 5.5, which was used for our following experiments. The primary purpose of the current work is to check the possibility of using the biofilm-infected 3D urothelial cell model for testing antimicrobial nanotherapeutics; the NPs were tested mainly about their essential characteristics as nanocarriers of the antifungal agent. These antifungal nanotherapeutics could be potentially changed into any other existing formulations.

The results obtained from the average hydrodynamic diameter and zeta-potential analysis of the produced shellac NPs as a function of Fluconazole concentration at pH 5.5 are shown in Figure 5. The increase of the Fluconazole concentration had only a very minor effect on the average nanoparticle hydrodynamic diameter, ranging between 68 nm to 79 nm.

The encapsulation of the antifungal agent, Fluconazole, was achieved by pH drop. The mixture of 0.2 wt% ammonium shellac (Aqua Gold), 0.25 wt% P407, and 0.02 wt% Fluconazole was fully soluble at pH 10 after sonication. The NPs precipitated after the pH was altered to 4, which intercalated the Fluconazole inside their shellac cores. The NPs were collected by centrifugation and used as 1×stock nanosuspension. The encapsulation efficiency of the NPs was detected by a UV-visible spectrometer at 260 nm as a function of time and pH. The pH of the stock 1× nanosuspension was changed by dropwise addition of 0.25M HCl and 0.25M NaOH, and then the solution was pelletized to collect the supernatant for encapsulation test. The remaining Fluconazole in the supernatant was regarded as nonencapsulated.

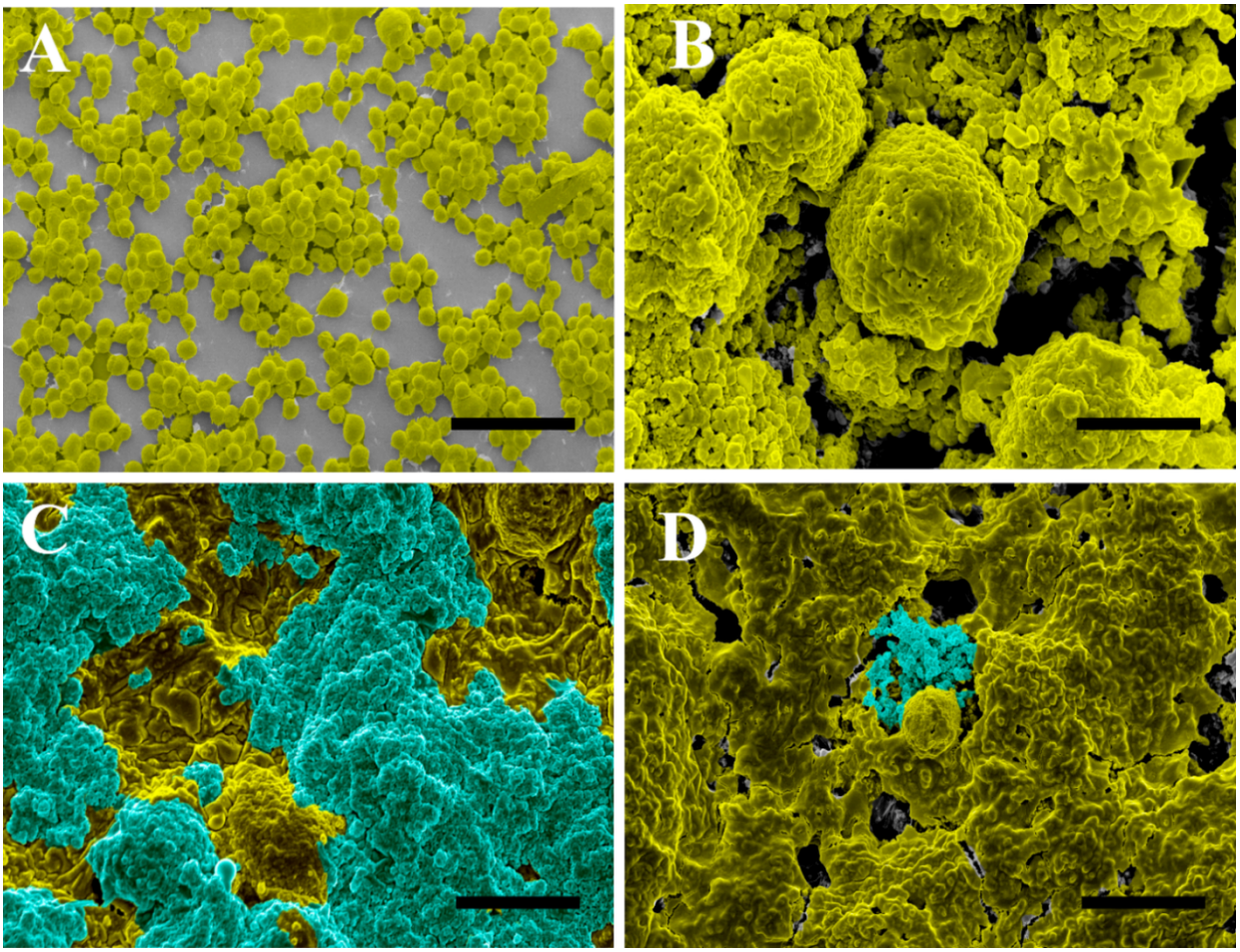

Figure 9. False colour SEM images of A: a layer of individual ECV 304 cells without any fungal infection or treatment by 4× Lyzozyme-coated Fluconazole-loaded Shellac NPs stock solution. B: Individual ECV 304 clusteroids layer without fungal infection or Lyzozyme-coated Fluconazole-loaded Shellac NPs treatment. C: ECV 304 clusteroid layer infected with Candida. albicans biofilm. D: ECV 304 clusteroid layer infected with *C. albicans* biofilm imposed by the treatment of Lyzozyme-coated Fluconazole-loaded Shellac NPs stock formulation. The bar is 100 µm for (A, B, C,) and 200 µm for (D). The 1× stock suspension of the Lysozyme-coated Fluconazole-loaded Shellac NPs is 0.2 wt% Shellac, 0.25 wt% P407, 0.2 wt% Lysozyme and 0.02 wt% Fluconazole. The cell concentration used in the experiments was 1×10^5/mL. Yellow colour represents the ECV 304 cell clusteroids while green colour represents the *C. albicans* biofilm. The original SEM images are shown in Figure S2.

As can be seen from Figure 6, the pH had only a minor effect on the Fluconazole encapsulation efficiency. All the set groups yielded an encapsulation efficiency higher than 70 %. The release kinetics of the Fluconazole from the NPs 1×stock sususpension was measured at pH 5.5 as a function of time. Figure 6 shows that the Fluconazole released about 50 % after 15 h and approximately 70 % after 25 h. This release kinetics is ideal for treating the biofilms. The SEM observation correlated to the results from the Malvern Nanosizer (Figure 7). The NPs had a spherical shape and were about 60-90 nm

in size. The zeta-potential was influenced by the Fluconazole with no more than 30% variation. The negative surface charging remained in all the set groups since the residual─COOH groups of the shellac components (shelloic acids).

The efficiency of the lysozyme-coated Fluconazole-loaded NPs treatment for clearance the Candida biofilm on 3D layer of Clusteroids

Here we examined with the antifungal activity of the Lysozyme-coated Shellac nanocarriers of Fluconazle on the biofilm anchored on the 3D layer of urothelial clusteroids. To determine the efficiency of the biofilm clearance of the NPs, different concentrations of stock solutions were applied on the *C. albicans* biofilm infected 3D layer of ECV 304 cell clusteroids.

As could be seen in Figure 8A, the increased concentration of the NPs delivered higher efficiency on clearing of the fungal biofilm, with a 5 log reduction on the overall amount of the viable fungal cells when treated with 4× stock solution of the NPs. The lower NPs concentration were not enough to clear the whole fungal biofilm. This might be attributed to the intrinsic high resistance of the *C. albicans* to Fluconazole. The individual components of the NPs were also separately tested on their efficiency of biofilm clearance with equal concentration to the oe used in the NPs. Figure 8B demonstrated that the major contributor to the antifungal action was brought by the Fluconazole payload. The Lysozyme also showed a certain fungal killing effect, as it can catalyze the hydrolysis of 1,4-beta-linkages between N-acetylmuramic acid and N-acetyl-D-glucosamine residues in peptidoglycans. The other components of the NPs showed very limited positive effects on biofilm clearance.

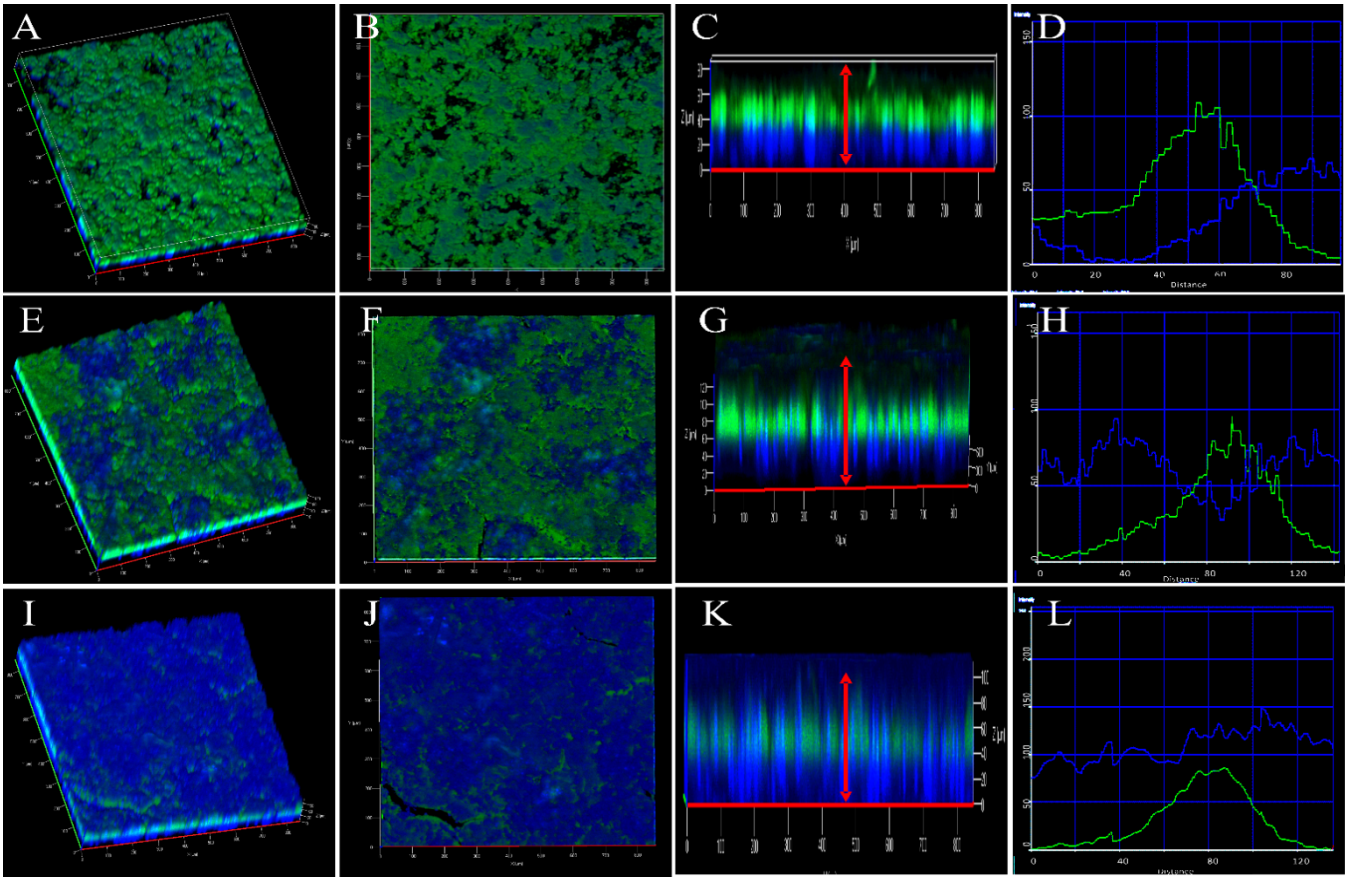

Figure 10. Confocal laser scanning microscope observation of biofilm/ECV 304 clusteroids co-cultures before(A, B, C), after 12 h (E, F, G) and 24 h (I, J, K) the treatment of 4×stock solution of the NPs. 50 μm for D-J. The fluorescence intensity of Figures C, G, K is displayed in Figures D, H, L, respectively. The size of the box is 800 μm×800 μm×80 μm(X, Y, Z). The concentration of the 1×stock solution of NPs is 0.2 wt% Shellac, 0.25 wt% P407, 0.2 wt% Lysozyme and 0.02 wt% Fluconazole. The fluorescence intensity was measure by ZEN software(Blue edition). The red arrows indicate where the fluorescence intensity was measured.

SEM imaging was employed to examine the microstructure of the fungal biofilm infection on the 3D layer of clusteroids (Figure 9). The biofilm was manually adjusted to green color, and the cells were painted yellow. The SEM images shows clearly the morphology of the biofilm stuck on the cell clusteroids layer (Figure 9C, D). After the treatment of the NPs, only a few planktonic fungal cells could be observed. The original images of the SEM were provided in Figure S2.

It is worth mentioning that none of the individual components of the nanocarrier could match the biofilm clearing efficiency of the composite NPs, which dominated the effect of the individual components. These results indicates the synergistic effect of the nanoformulation in killing the *C. albicans* cells and clearing the fungal biofilm. To facilitate the monitoring of the biofilm removal, the biofilm clearing process of the 4× stock NPs solution was visualized using CLSM observations. The 3D layer of clusteroids was pre-stained with DAPI dye before the fungal biofilm infection, which was

contrast-stained with CFSE (generational dye). The removal of the biofilm was partly achieved after 1 h of incubation starting from the outer layer of the biofilm (Figure 10A-D). The CFSE fluorescence signal was slightly reduced. After 12 h of incubation with the NPs treatment half of the biofilm deposited on the surface of the clusteroids peeled off (Figure10 E-H). After 24 h incubation, the biofilm initially attached to the surface of the 3D clusteroids layer was mostly removed, only leaving a very low amount of fungal cells inside of the clusteroids layer (Figure 10 H-K). This could be proven by the fluorescence intensity that the signals peaked at the central area. The intractability of the complete removal of the biofilm is mainly derived from its thick EPS. The long-term release and the electrostatic absorbance of the NPs showed a positive synergistic effect on clearing the biofilm. lusteroids However, the images collected from CLSM observations demonstrated that the partly rough morphology of the 3D layer of clusteroids may potentially reduce the efficiency of the fungal biofilm removal. To clarify this point, cryostat sectioning was used to visualise whether the fungal cell infection in the core of the clusteroids was restrained. From Figure 11, one can see the junction of the clusteroids in the bright field observations. Similarly, the green fluorescence signal from the fungal cells, was reduced by over 60%. However, a minor residue of fungal cells could still be detected in the sectioning slice after the 4×stock solution treatment.

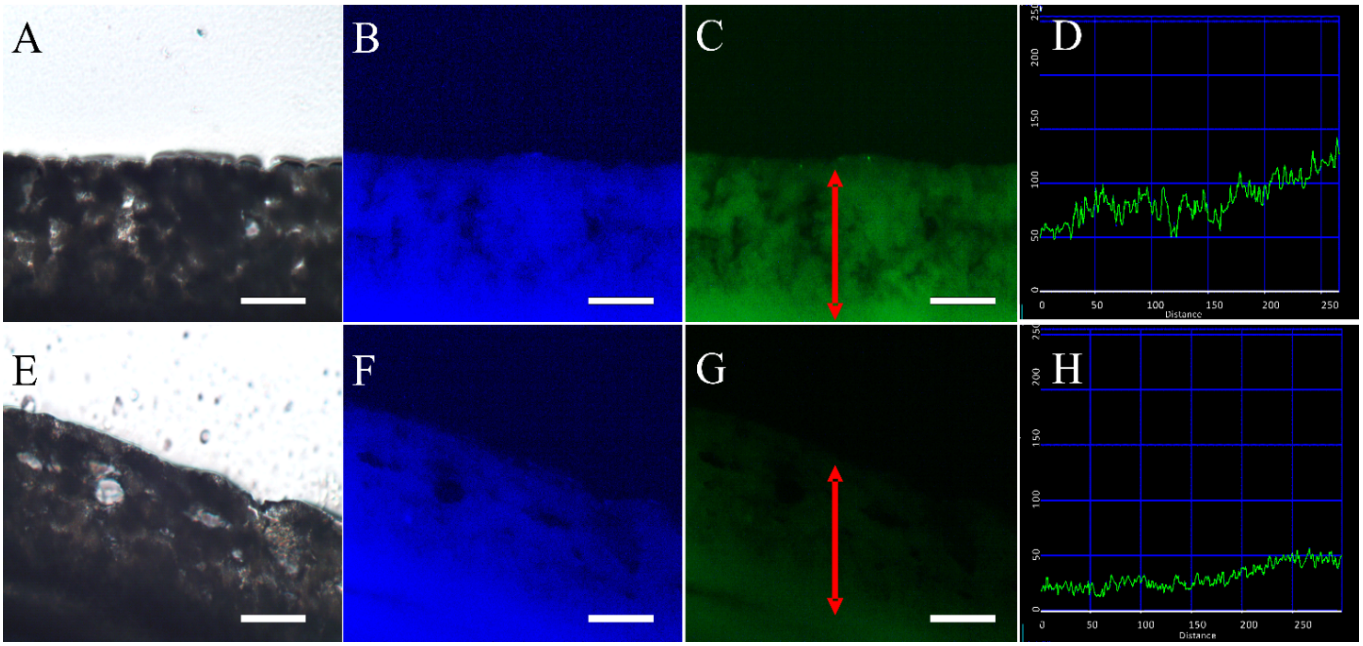

Figure 11. Microscopy observation of cryostat sectioning slices of the 3D co-cultured fungal biofilm infected clusteroids layer: before(A, B, C) and after(E, F, G) treatment with 4×stock solution. Each slice cutted by the cryo-sectioning is 10 µm. Olympus BX51 fluorescence microscope was used for the series observations. The fluorescence intensity of C and G was measure by ZEN software(Blue edition) and is shown in D and H. The bar is 100 µm (same for all images). The concentration of 1×stock solution is 0.2 wt% Shellac, 0.25 wt% P407-0.2 wt% Lysozyme and 0.02 wt% Fluconazole. The red arrows indicate where the fluorescence intensity was measured.

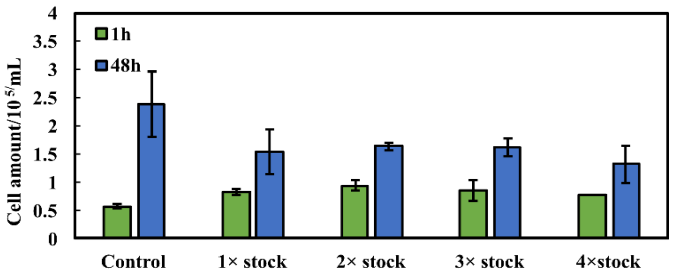

Figure 12. Cytotoxicy of different concentrations of Lysozyme-coated Fluconazole-loaded shellac NPs solutions on the proliferation of the 3D layers of ECV304 clusteroids after 1 h and 48 h culture. The cell numbers in the different cultures taken after 1 h and 48 h were calculated by standard curve.

Cytotoxicity of the NPs treatment on the ECV 304 clusteroids

NPs treatmnts of different concentration of the stock suspensions were added to the microwell plate containing the 3D cell clusteroids layer to investigate the cytotoxicity of the NPs on the ECV 304 cells. In clinical practice, the utilization of the NPs treatment would potentially affect the surrounding uninfected cells. To evaluate and potentially reduce this influence, the cytotoxicity test was carried out using an MTT assay. Figure 12 shows that 1×stock solution could reduce the overall cell amount by 40% after 48h. Interestingly, the cell proliferation was not impaired by the addition of the highly concentrated amount of the NPs (4×stock) which indicates a saturation. The 4×stock solution had only a negligible effect on ECV 304 cell viability. No significant difference was observed in ECV 304 cells amount after 1 h of treatment with different concentrations of the stock solution. Compared to the 5-log reduction in the *C. albicans* cells after 24h of treatment, only a 40% inhibition on ECV 304 cell proliferation clearly indicate that this NPs treatment as an efficient biofilm cleaning formulation.

Conclusions

Here we developed a *C. albicans* biofilm-infected 3D urothelial cell clusteroids model for mimicking the bladder inner cell wall. For clearing fungal biofilms on the 3D layer of urothelial clusteroids, we designed a Fluconazole-loaded shellac nanotherapeutic system using a coating of the cationic enzyme Lysozyme to functionalize the Fluconazole-nanocarriers. The cationic Lysozyme coating reversed the surface charge of the negatively charged Shellac NPs into a positively charged nanocarriers targeting the negatively charged *C. albicans* biofilm. The idea is that the Lysozyme-coating of the nanocarrier would partially digest the EPS of the biofilm which is rich in peptoglycans and facilitate the delivery of the antifungal agent Fluconazole to the encased *C. albicans* cells.

CLSM and SEM imaging, bright field microscopy, CFU counts, MTT assay, and cryostat sectioning were employed to characterise the state of the *C. albicans* biofilm infected 3D layer of urothelial clusteroids before and after the nanotherapy treatment. These antifungal NPs showed a significant enhancement of the biofilm clearing effect compared to any free individual components (Shellac, P407, or Fluconazole). The super-strong antifungal effect of this treatment did not significantlhy increase the cytotoxicity of the 3D clusteroid model; the treatment of the clusteroids brought minor effects on the clusteroids proliferation. The whole process of this work includes urothelial cell culture and formation of cell clusteroids, biofilm infection, and NPs treatment. Such a protocol could be potentially used as a general platform for

mimicking a wide range of fungal biofilm infections or bacterial infections on selected organs or body parts by replacing the species of cell type and pathogen type. Taken together, the introduced biofilm-infected 3D urothelial cell clusteroids platform is an ideal model for mimicking urinary tract infection. This platform provides researchers with a facile approach to test various therapeutics especially nanocarrier-based therapeutics, for biofilm clearance. This work would fill in the gaps in *in vitro* urinary models for biofilm infection and could be a useful guide for relevant biofilm *in vitro* simulations which expected to facilitate the clinical use of nanotechnology-based antimicrobial therapeutics.

Supplementary Information

The enclosed Electronic supplementary information file (ESI) contains tabulated data for Figure S1-5.

Conflicts of interest

There are no conflicts to declare.

Acknowledgments

A. W. thanks the Chinese Scholarship Council for the financial support of his Ph.D. studies. The authors would like to thank the SEM technician Mr Timothy Dunstan (University of Hull) for his assistance during this project.

ORCID IDs

Anheng Wang: 0000-0001-6616-2828

Paul J. Weldrick: 0000-0002-1791-5659

Leigh Madden: 0000-0002-1503-1147

Vesselin N. Paunov: 0000-0001-6878-1681

References

1 J. Kaufman, M. Temple-Smith and L. Sanci, *BMJ Paediatr. Open*, 2019, **3**, e000487.

2 P. Yousefi, A. Cyrus, Z. Moghaddasi, F. Dorreh and A. Aravand, *J. Adv. Med. and Biomed*. Res., 2011, **19**, 66-76.

3 K. Gupta, L. Grigoryan and B. Trautner, *Ann. Intern. Med.*, 2017, **167**, ITC49-ITC64.

4 T. M. Hooton, J. *Antimicrob. Chemother*., 2000, **46** Suppl 1, 1-7; discussion 63-5.

5 K. Gupta, T. M. Hooton, K. G. Naber, B. Wullt, R. Colgan, L. G. Miller, G. J. Moran, L. E. Nicolle, R. Raz, A. J. Schaeffer, D. E. Soper, *Clin. Infect. Dis*., 2011, **52**, e103-20.

6 C. W. Tan and M. P. Chlebicki, *Singapore Med. J*., 2016, **57**, 485-490.

7 F. Wagenlehner and K. Naber, *J. Hosp. Infect*., 2000, **46**, 171-181.

8 J. R. Phillips and M. G. Karlowicz, *Pediatr. Infect. Dis. J*., 1997, **16**, 190-194.

9 E. H. Elpern, K. Killeen, A. Ketchem, A. Wiley, G. Patel and O. Lateef, *Am. J. Crit. Care*, 2009, **18**, 535-41; quiz 542.

10 S. Niveditha, S. Pramodhini, S. Umadevi, S. Kumar and S. Stephen, *J. Clin. Diagn. Res*., 2012, **6**, 1478-1482.

11 H. Pelling, J. Nzakizwanayo, S. Milo, E. L. Denham, W. M. MacFarlane, L. J. Bock, J. M. Sutton and B. V. Jones, *Lett. Appl. Microbiol*., 2019, **68**, 277-293.

12 N. S. Morris, D. J. Stickler and R. J. McLean, *World J. Urol*., 1999, **17**, 345-350.

13 S. P. Hawser and L. J. Douglas, *Infect. Immun*., 1994, **62**, 915-921.

14 J. Chandra, D. M. Kuhn, P. K. Mukherjee, L. L. Hoyer, T. McCormick and M. A. Ghannoum, *J. Bacteriol.*, 2001, **183**, 5385-5394.

15 D. Davies, *Nat. Rev. Drug Discov*., 2003, **2**, 114-122.

16 G. O'Toole, H. B. Kaplan and R. Kolter, *Annu. Rev. Microbiol*., 2000, **54**, 49-79.

17 M. G. Trulear and W. G. Characklis, *J. Water Pollut. Control Fed*., 1982, 54, 1288-1301.

18 K. Lewis, *Antimicrob. Agents Chemother*., 2001, 45, 999-1007.

19 H.-C. Flemming and J. Wingender, *Nat. Rev. Microbiol*., 2010, **8**, 623-633.

20 L. Robino and P. Scavone, *Future Microbiol*., 2020, **15**, 377-379.

21 Y. Liu, L. Shi, L. Su, H. C. van der Mei, P. C. Jutte, Y. Ren and H. J. Busscher, *Chem. Soc. Rev.*, 2019, **48**, 428-446.

22 E. N. Taylor, K. M. Kummer, D. Dyondi, T. J. Webster and R. Banerjee, *Nanoscale*, 2014, **6**, 825-832.

23 F. Haghighi, S. R. Mohammadi, P. Mohammadi, M. Eskandari and S. Hosseinkhani, *Bratisl. Lek. Listy*, 2012, **113**, 707-711.

24 S. M. Abdelghany, D. J. Quinn, R. J. Ingram, B. F. Gilmore, R. F. Donnelly, C. C. Taggart and C. J. Scott, *Int. J. Nanomedicine*, 2012, **7**, 4053-4063.

25 K. Qvortrup, L. D. Hultqvist, M. Nilsson, T. H. Jakobsen, C. U. Jansen, J. Uhd, J. B. Andersen, T. E. Nielsen, M. Givskov and T. Tolker-Nielsen*, Front. Chem*., 2019, **7**, 742.

26 P.J. Weldrick, M.J. Hardman and V.N. Paunov, *Mater. Chem. Front.*, 2021, **5**, 961-972.

27 A. Wang, P. J. Weldrick, L.A. Madden and V.N. Paunov, *ACS Appl. Mater. Interf*., 2021, **13**, 22182–22194.

28 P. J. Weldrick, M. J. Hardman and V. N. Paunov, *ACS Appl. Mater. Interf*., 2019, **11**, 43902-43919.

29 A. F. Halbus, T. S. Horozov and V. N. Paunov, *ACS Appl. Mater. Interf*., 2019, **11**, 12232-12243.

30 P. J. Weldrick, S. Iveson, M. J. Hardman and V. N. Paunov, Nanoscale, 2019, **11**, 10472-10485.

31 D. Huh, G. A. Hamilton and D. E. Ingber, *Trends Cell Biol*., 2011, **21**, 745-754.

32 M. Ravi, V. Paramesh, S. R. Kaviya, E. Anuradha and F. D. P. Solomon, *J. Cell. Physiol*., 2015, **230**, 16-26.

33 O. Chaudhuri, *Biomater. Sci*., 2017, **5**, 1480-1490.

34 V. van Duinen, S. J. Trietsch, J. Joore, P. Vulto and T. Hankemeier*, Curr. Opin. Biotechnol*., 2015, **35**, 118-126.

35 A. Wang, L. A. Madden and V. N. Paunov, *J. Mater. Chem. B*., 2020, **8**, 10487-10501.

36 A. A. K. Das, B. W. Filby, D. A. Geddes, D. Legrande and V. N. Paunov, *Mater. Horiz*., 2017, **4**, 1196-1200.

37 S. B. G. Celik, S. R. Dominici, B. W. Filby, A. A. K. Das, L. A. Madden and V. N. Paunov, *Biomimetics*, 2019, **4**, 50.

38 A. Wang, L. A. Madden and V. N. Paunov, *Mater. Adv*., 2020, **1**, 3022-3032.

39 Z. Khatoon, C. D. McTiernan, E. J. Suuronen, T.-F. Mah and E. I. Alarcon, *Heliyon*, 2018, **4**, e01067.

40 S. Veerachamy, T. Yarlagadda, G. Manivasagam and P. K. Yarlagadda, *Proc. Inst. Mech. Eng. H*, 2014, **228**, 1083-1099.

41 W. Fu, T. Forster, O. Mayer, J. J. Curtin, S. M. Lehman and R. M. Donlan, *Antimicrob. Agents Chemother*., 2010, **54**, 397-404.

42 A. E. Hodgson, S. M. Nelson, M. R. W. Brown and P. Gilbert, J. *Appl. Bacteriol*., 1995, **79**, 87-93.

43 K. Marion-Ferey, M. Pasmore, P. Stoodley, S. Wilson, G. P. Husson and J. W. Costerton, *J. Hosp. Infect*., 2003, **53**, 64-71.

44 C. Badet, A. Furiga and N. Thébaud, *Oral Health Prev. Dent*., 2008, **6**, 337-341.

45 K. E. Hill, S. Malic, R. McKee, T. Rennison, K. G. Harding, D. W. Williams and D. W. Thomas, *J. Antimicrob. Chemother*., 2010, **65**, 1195-1206.

46 S.S.M, Al-Obaidy, G.M. Greenway and V.N. Paunov, *Nanoscale Adv*., 2019, **1**, 858–872.

47 S.S.M. Al-Obaidy, A.F Halbus, G.M. Greenway and V.N. Paunov, J. *Mater. Chem. B*, 2019, **7**, 3119-3133.

48 A.P. Richter, J.S. Brown, B. Bharti, A. Wang, S. Gangwal, K. Houck, E.A. Cohen Hubal, V.N. Paunov, S.D. Stoyanov, O.D. Velev., *Nat. Nanotechnol.*, 2015, **10**, 817−823.

49 M.J. Al-Awady, A. Fauchet, G.M. Greenway, V.N. Paunov, *J. Mater. Chem. B*, 2017, **5**, 7885-7897.

50 M. Al-Awady, P. J. Weldrick, M.J. Hardman, G. M. Greenway and V.N. Paunov, *Mater. Chem. Front.*, 2018, **2**, 2032-2044.

51 A.F. Halbus, T.S. Horozov and V.N. Paunov, *Biomimetics*, 2019, **4**, 1-20.

52 A.F. Halbus, T.S. Horozov and V.N. Paunov, *Nanoscale Adv.*, 2019, **1**, 2323-2336.

53 M.J. Al-Awady, G.M. Greenway, V.N. Paunov. *RSC Adv*., 2015, **5**, 37044–37059.